Sensing and Bio-Sensing Research 3 (2015) 7–11

Contents lists available at ScienceDirect

Sensing and Bio-Sensing Research

journal homepage: www.elsevier.com/locate/sbsr

Facile fabrication of 3D layer-by-layer graphene-gold nanorod hybrid architecture for hydrogen peroxide based electrochemical biosensor

Chenming Xue [a], Chih-Chien Kung [b], Min Gao [a], Chung-Chiun Liu [b], Liming Dai [c], Augustine Urbas [d], Quan Li [a,*]

[a] Liquid Crystal Institute and Chemical Physics Interdisciplinary Program, Kent State University, Kent, OH 44242, USA
[b] Department of Chemical Engineering, Case Western Reserve University, Cleveland, OH 44106, USA
[c] Department of Macromolecular Science and Engineering, Case Western Reserve University, Cleveland, OH 44106, USA
[d] Materials and Manufacturing Directorate, Air Force Research Laboratory WPAFB, OH 45433, USA

ARTICLE INFO

Keywords:
Gold nanorod
Graphene
3D hybrid nanostructure
H_2O_2 detection
Biosensor

ABSTRACT

Three-dimensional (3D) layer-by-layer graphene-gold nanorod (GNR) architecture has been constructed. The resulting hybrid nanomaterials' architecture has been tested for detecting hydrogen peroxide (H_2O_2) through the electrocatalytic reaction on a three electrode disposable biosensor platform. Cyclic voltammetry and amperometry were used to characterize and assess the performance of the biosensor. The 3D layer-by-layer modified electrode exhibited the highest sensitivity compared to the active carbon, graphene-oxide, cysteine-graphene oxide and GNR coated electrodes. This research explored the feasibility of using the 3D hybrid graphene-GNR as a template for biosensor. The 3D hybrid structure exhibited higher sensitivity than GNRs alone. SEM showed the explanation that GNRs had self-aggregates reducing the contact surface area when coated on the active carbon electrode, while there were no such aggregates in the 3D structure, and TEM illustrated that GNRs dispersed well in the 3D structure. This research demonstrated a better way to prepare well-separated metal nanoparticles by using the 3D layer-by-layer structure. Consequently, other single and bi-metallic metal nanoparticles could be incorporated into such structure. As a practical example, 3D layer-by-layer nanomaterials modified active carbon electrode was used for detecting glucose showing very good sensitivity and minimum interference by ascorbic acid and uric acid in test solution, which indicated a good selectivity of the biosensor as well.

1. Introduction

Electrochemical biosensors are highly effective in detecting biomolecules due to the high sensitivity, real-time monitoring capability and low cost, compared to the relatively complex and expensive measurement techniques such as radioisotope tracing, NMR spectroscopy, and microfluorometry assay [12,25,18]. In recent years, electrochemical biosensors based on the enzymatic activity have received increasing interest, for its advantages of low cost, portability, fast response time, and ease-of-usage by non-specialist personnel [3]. Hydrogen peroxide (H_2O_2) is an electrochemical active species produced by various oxidase enzymes. Thus, the measurement of H_2O_2 in various enzymatic reactions can quantify the analyte for biomarker detections as shown in Eq. (1) [11]. The use of electrode or catalyst-modified electrode as a transducer was based on Eq. (2) of oxidation of H_2O_2:

$$\text{Analyte} + O_2 \xrightarrow{\text{oxidase}} \text{byproduct} + H_2O_2 \quad (1)$$

$$H_2O_2 \xrightarrow{\text{elecrode}} O_2 + 2H^+ + 2e^- \quad (2)$$

However, the total sensitivity of biosensors based on traditional materials is hindered due to restrictions in mass transport, enzyme loading, and electrochemical coupling, limiting the potential for miniaturization. This affects the limitation of detection of the analyte as well. Unconventional nanomaterials with good biocompatibility and electrocatalytic activities have been widely incorporated in biosensors to overcome these shortcomings [13,6,16,21].

Metal nanoparticles (NP), particularly Au and Pt, have been used in the development of electrochemical sensors and biosensors based on their catalytic activities [31,21]. They have the advantages of large surface-to-volume ratio and special binding site on the surface of nanoparticles, which lead to a fast communication between an enzymatic process and a nanoparticle response for signal transduction in biosensing or for catalytic reactions [2].

* Corresponding author.
E-mail address: qli1@kent.edu (Q. Li).

http://dx.doi.org/10.1016/j.sbsr.2014.10.008
2214-1804/

PtNPs has superior sensitivity because of its enhanced electron transfer and reduction of overpotential for H_2O_2 oxidation [9,30]. However, electrodes modified with pure PtNPs requires a relatively high electrochemical potential (ca. +0.7 V versus Ag/AgCl) to oxidize H_2O_2 generating the oxidation current. At relatively high potential, it will oxidize ascorbic acid (AA) and uric acid (UA) in human blood resulting in an interference of the detection of the analyte (e.g. glucose) [4]. Hence, gold nanoparticles (GNPs) are considered to be another potential candidate based on its good performance in H_2O_2 related sensors with lower potential [5]. Different from spherical GNP, gold nanorods (GNR) introduces more interesting functions based on its anisotropic shape having unique localized surface plasmon resonance (LSPR), which brings applications in cancer diagnosis and monitoring local environment changes [8,1]. This can potentially expand the diversity of biosensors. However, owing to its anisotropic shape, GNR tends to self-aggregate during surface processing forming side-by-side assemblies [19,27] Therefore, it is desirable to introduce selected conducting materials to support the GNR in order to induce decent dispersity.

Carbon nanomaterials are excellent candidates as the supporting materials for metal NPs due to their unique structural, electrical, and mechanical properties [20,22]. The carbon nanomaterials can enhance the available electrochemical active surface area of electrocatalyst and provide high mass transport of reactants to the electrocatalyst. Among these carbon materials, graphene is a two dimensional monolayer of carbon atoms with high surface area, chemical stability, and thermal stability, making it as a useful substrate for electronics [24]. However, graphene sheets are difficult to exfoliate because their planar polycyclic aromatic structures favor tight packing as a result of strong π–π interactions. Also, even the graphene sheets are destacked, they can only support metal NPs on its two sides and these individual graphene-metal NP hybrid structures may lack connection to each other. Therefore, it requires a 3D structure to enhance the loading of metal NPs and interconnection between the metal NPs. In our previous work, a 3D graphene-GNR layer-by-layer nanostructure was constructed [28]. The GNRs dispersed well and linked the conductive reduced graphene layers through stable covalent Au-S bond in this 3D structure. Therefore, this architecture possesses ideal large surface area and conductive pathways for biosensing.

In this study, the prepared 3D layer-by-layer graphene-GNR hybrid nanomaterial was coated on a thick film screen-printed active carbon powder electrode as a single-use, disposable biosensor for testing H_2O_2. The performance of GNR without supporting graphene layers was tested for comparison through electrochemical analytical techniques, such as cyclic voltammetry (CV) and amperometric measurements. The interference test was executed by detecting glucose in the presence of AA and UA showing the selectivity performance of this biosensor.

2. Experimental

2.1. Materials and instruments

All chemicals and solvents were purchased from commercial suppliers and used without further purification. $HAuCl_4$ was 30 wt% in diluted HCl solution. UV–visible spectra were collected on a PerkinElmer Lambda 25 UV–Vis spectrometer at the resolution of 1 nm. For transmission electron microscopy (TEM) observation, solution samples were first dispersed on TEM Cu grids pre-coated with thin holey carbon film (Cu-400 HN) purchased from Pacific Grid Tech. After completely dried, they were digitized using a FEI Tecnai TF20 FEG TEM equipped with a Gatum 4 k UltraScan CCD camera. For scanning electron microscopy (SEM), it was obtained in a FEI Quanta 450 FEG SEM. All the experiments were conducted at room temperature. Phosphate buffer solution (PBS) (0.1 M) of pH 7.4 solution was prepared with 0.15 M KCl as the supporting electrolyte, and KH_2PO_4, K_2HPO_4, and deionized water were used in appropriate portions.

2.2. Preparation of the 3D layer-by-layer hybrid structure

The 3D layer-by-layer nanostructure was prepared as described in supporting information. The characterization of the 3D layer-by-layer structure will be discussed in Section 3.1. Fig. 1 shows steps of the synthesis of this 3D layer-by-layer hybrid structure.

2.3. Electrochemical measurements

Prior to experiments, PBS was first deoxygenated with nitrogen gas. The structure and dimensions of this biosensor prototype is shown in Fig. 2. Solutions of GO, GO-Cys, GNR, GO-Cys-GNR were drop cast on the working electrode. During preparation, the concentration of GNRs in solutions of GNR and GO-Cys-GNR was maintained same (ca. 0.02 mg/ml). After drying, PBS solution containing various amount of H_2O_2 was drop casted (6 μl) on the center part covering all the electrodes. A work station (CHI 660C, CH Instrument, Inc., Austin, TX) was used for cyclic voltammetry and amperometry investigations. Cyclic voltammetric studies were arranged over a voltage range of −0.2 V to + 1.2 V versus Ag/AgCl reference with a voltage scan rate of 0.1 V/s.

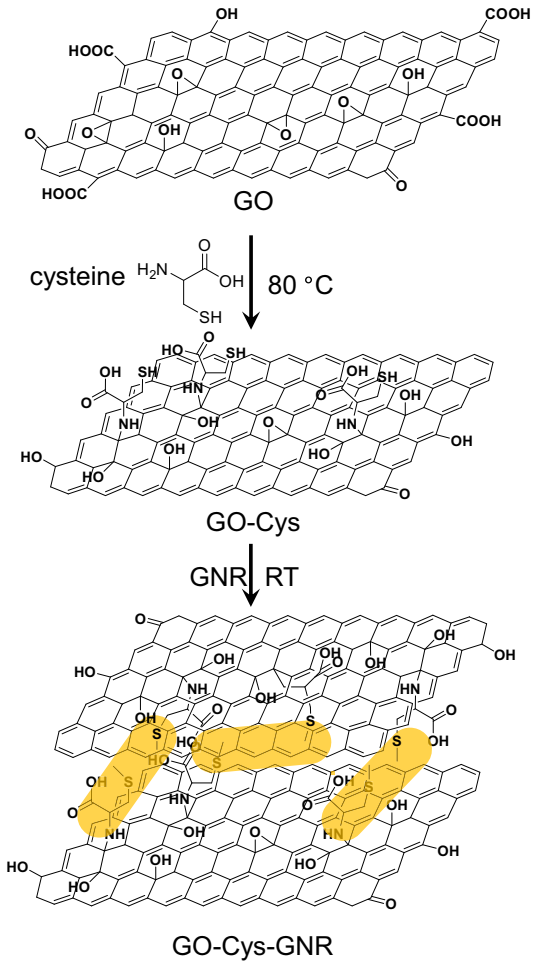

Fig. 1. Fabrication of 3D layer-by-layer hybrid structure.

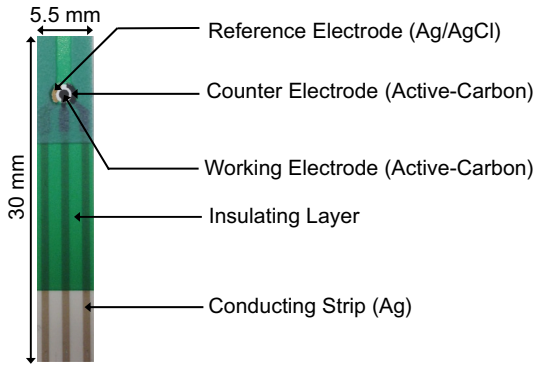

Fig. 2. The electrode structure and dimensions of the biosensor.

3. Results and discussion

3.1. Characterization of 3D GO-Cys-GNR nanohybrid

In Fig. 1, the functionalization of GO and subsequent preparation of 3D layer-by-layer graphene-GNR (GO-Cys-GNR) hybrid nanostructure are depicted. The experimental details are provided in supporting information. When the primary amine reacts with GO, there might be multiple reactions occurring simultaneously. Consequently, the major reaction under this condition involved the amine groups opening the epoxy groups through easy ring-opening reaction. A possible reaction mechanism was ascribed to nucleophilic attack at the α-carbon by the primary amine, leaving an open hydroxyl group. This had been demonstrated in the reaction of GO with octadecylamine [23,29]. After the preparation of GO-Cys, GNRs were added to attach onto GO-Cys layers via Au-S linkages. Anisotropic GNRs: 14.6 × 44.3 nm was used in this process. This average size of GNRs was based on counting 500 individual nanoparticles. Before adding GNRs, GO-Cys could not fully precipitate during centrifugation due to its relatively light weight, leaving a dark black solution as the top layer. After adding GNRs the assembled hybrid structures were heavier, and most of the GO-Cys then precipitated in the bottom during centrifugation, leaving a colorless top layer solution. The synthesis was also traced by UV–vis spectra as shown in Fig. S1. Pristine GO showed a typical absorption peak at 230 nm and this peak shifted to 253 nm after reaction with cysteine, which was similar to other reduction reaction [15] Typical LSPR of GNRs appeared after further combining with GO-Cys. There appeared peaks at ca. 520 nm and a peak at 705 nm, corresponding to the transverse and longitudinal LSPR respectively.

The critical role of cysteine in the successful binding of GNRs and GO was confirmed by TEM and is shown in Fig. S2. To confirm GNRs reacted with GO-Cys in solution, a reference sample was prepared by mixing GNRs with pristine GO solution under the same condition. A droplet of each mixture was deposited on a holey lacey carbon coated TEM grid. Suspended films could be observed on some of the holes of the grid. Fig. S2A shows that without the linking thiol group provided by cysteine, the GNRs tend to aggregate and do not disperse well. In contrast, for 3D layer-by-layer structure, the GNRs are attached to the GO-Cys in a uniform well-dispersed manner (Fig. S2B).

The structure of GO changed after functionalization with cysteine, the GO and GO-Cys were analyzed by Raman, XPS, and molecular simulation in our previous reported study [28]. The 3D layer-by-layer hybrid architecture was characterized and confirmed by TEM by tilting the carbon film coated samples as shown in Fig. 3.

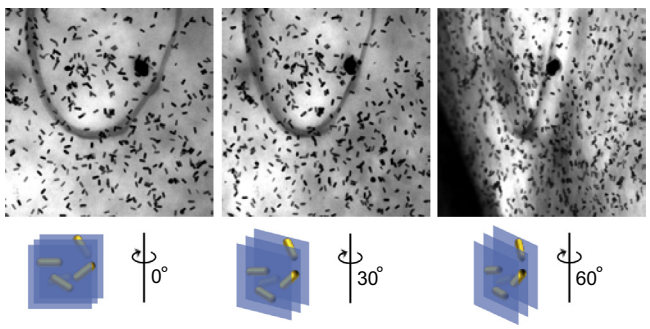

Fig. 3. Illustration of 3D GO-Cys-GNR by tilting in TEM, below is the schematic description of the 3D layer-by-layer structure during tilting. The grey arc in TEM images is from holey carbon films coated on TEM grids.

3.2. Electrochemical characterization and performance

The electrochemical performance of the thick film screen-printed active carbon working electrode coated with GO, GO-Cys, GNR, GO-Cys-GNR were investigated by CV using PBS containing H_2O_2 (0.1 mM) as the benchmark redox reactions [26]. Enzymatic produced H_2O_2 shown in Eq. (1) was oxidized at an appropriate electrochemical potential. The oxidation current of the generated H_2O_2 quantified the concentration of the analyte stochiometrically. In order to assess the modified working electrodes for the detection of H_2O_2, experiments were conducted by measuring H_2O_2 (0.1 M) in pH 7.4 PBS with KCl as a supporting electrolyte. The scanned potential range was between −0.2 V and +1.2 V versus SCE for 10 cycles with a voltage scan rate of 0.1 V/s.

As shown in Fig. 4, the current densities for pure active carbon electrode and coated with GO and GO-Cys carbon electrode were relatively low. However, the GNRs and GO-Cys-GNRs coated carbon working electrodes exhibited significantly increases in current densities. This suggested that metal NPs-based sensor electrodes gave increased current response, and with higher sensitivity and selectivity for H_2O_2 sensing [7,4]. The reduction peaks appeared at 0.3 V for the GNR and GO-Cys-GNR electrodes as shown in Fig. 4, indicated enhanced electron and mass transfer due to the increased surface area and lower electric resistance of these modified electrodes. Based on the same weight percent of GNR used, the 3D GO-Cys-GNR showed a better electrochemical performance and this was ascribed to the potentially increased contact area of GNRs within.

3.3. Amperometric measurement of H_2O_2

The performances of the modified active carbon electrode were also evaluated by the amperometric detections of H_2O_2. Fig. S3 shows the amperometric responses of these modified electrodes

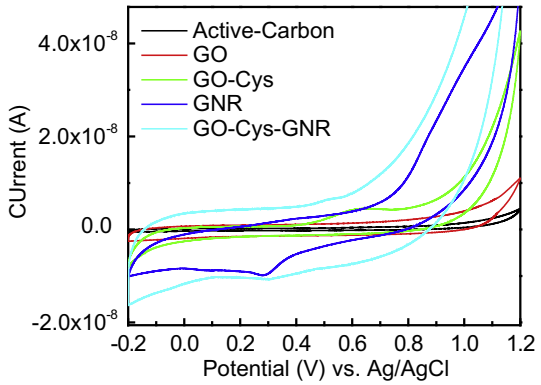

Fig. 4. Cyclic voltammograms of different materials coated on working electrodes (active carbon, GO, GO-Cys, GNR and GO-Cys-GNR) in the PBS (pH = 7.4) solution containing 0.1 mM H_2O_2 at a scan rate of 0.1 V/s.

at different H_2O_2 concentrations in PBS over the concentration range of 0-0.5 mM H_2O_2. The electrodes coated with GNR and GO-Cys-GNR show enhanced oxidation current outputs resulting by the relatively good electronic conductivity and good catalytic activity contributed by GNRs. The applied potential is +0.35 V versus Ag/AgCl. A stable steady-state amperometric response was obtained at 120 s. For GNR and GO-Cys-GNR modified electrodes, further studies on H_2O_2 detections were undertaken. Two ranges of H_2O_2 concentrations, 0–0.04 mM, and 0–5.0 mM were used based on the physiological meaningful detection range of H_2O_2 [14]. Fig. 5 shows the experimental results. Both GNR and GO-Cys-GNR modified electrodes showed improved performance compared to pure active carbon electrode. At lower H_2O_2 concentration range, the GNR amperometric sensor responded rapidly achieving 90% of the steady-state current within 10 s in average while the GO-Cys-GNR took longer time to reach stable state. Fig. S4 shows the current output of GNR and GO-Cys-GNR modified electrodes responding to H_2O_2 was linear over a low H_2O_2 concentration range. There were good linear relationships between the current outputs of the biosensor and H_2O_2. The sensitivity and the detection limit (LOD) were 0.418 μA mM^{-1} cm^{-2}, 2.9 μM for GNR, and 0.648 μA mM^{-1} cm^{-2}, 2.9 μM for GO-Cys-GNR, respectively. The LOD was calculated based on the signal to noise ratio (S/N = 3). GO-Cys-GNR showed higher sensitivity, which indicated a better performance in H_2O_2 sensing.

The GO-Cys-GNR exhibited a larger current output than GNR but a slower response to reach the stable state. This was due to the 3D structure which could increase the GNR surface area by preventing self-assembling, whereas it required longer time for H_2O_2 in solution to diffuse onto the GNRs, particularly those inside the 3D structure as illustrated in Fig. 6. Fig. 6 also shows the SEM of these two electrodes coated by GNRs and Go-Cys-GNR. Different surface structures were obvious. GNRs showed intensive aggregates when coated on the carbon electrode. There were no GNR aggregates in GO-Cys-GNR as GNRs were dispersed inside the 3D structure. The pieces of graphene sheets and the spread a few GNRs on the surface could be observed.

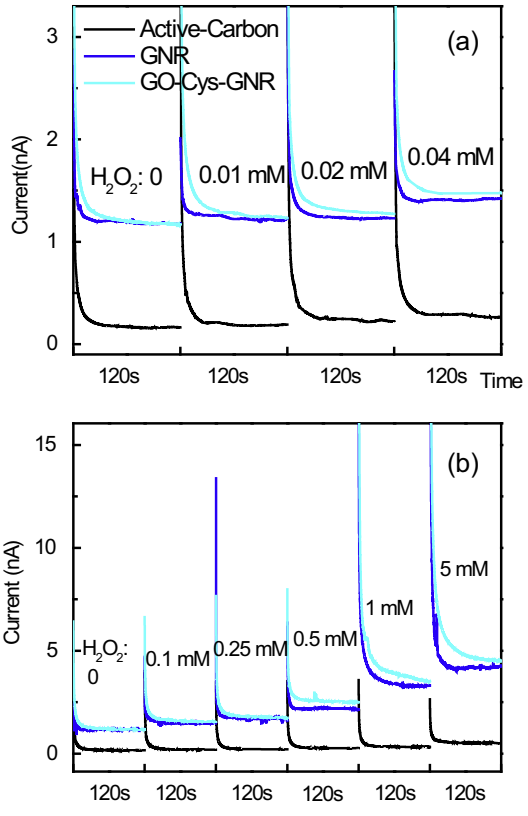

Fig. 5. The current-time response curves of active carbon, GNR and GO-Cys-GNR upon different concentration of H_2O_2 in PBS solution with more detailed study. (Repetition: $n = 3$).

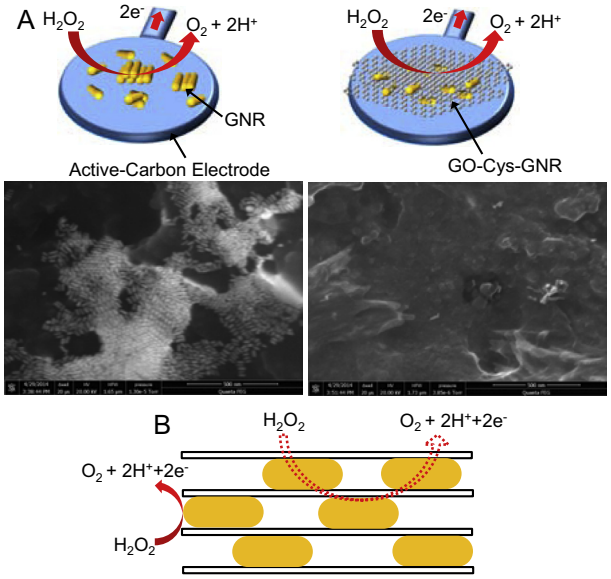

Fig. 6. (A) The schematic depiction and SEM observation of GNR (left) and GO-Cys-GNR (right) on the carbon electrodes. (B) The GNRs inside the 3D layer-by-layer hybrid structure took longer time to contact with H_2O_2 in solution.

Compared to other biosensors e.g. ([14]), the current intensity is very low here. To explain this, one reason is ascribed to the low concentration of GNRs and graphene materials in solution (see supporting information). For the second reason, the resistance of the electrodes and coated materials are high: the resistance of the active carbon electrode and its coated with different materials were showed in Fig. S5, *X* indicated the measuring of different materials with a certain distance. For each sample five measurements were performed. Since the whole electrode with a long Ag strip has a high resistance of 0.68 kΩ, the overall current intensity is much lower than that of directly used glassy carbon electrode [14]. Compared to GNR, 3D GO-Cys-GNR had a lower average resistance, and a smaller standard deviation for 5 measurements: GO-Cys-GNR: 254 Ω, 69 and GNR: 673 Ω, 203, respectively. This is because GNR had assemblies with poor dispersion on the electrode, whereas GO-Cys-GNR was much uniform showing better conductivity and lower standard deviation.

3.4. Interference tests

Glucose is one of the important biochemical substrates for cellular catabolism, and glucose biosensors based on enzymatic recognition by glucose oxidase have been extensively used in diabetes diagnostics [10] and β-cell physiology study [17] However, the potential interferences from other physiological species such as ascorbic acid (AA) and uric acid (UA) are always a concern for H_2O_2 based electrochemical biosensors. The typical physiological concentration of glucose in human blood is 4-5 mM, and of AA and UA in human blood are 0.125 mM and 0.33 mM, respectively [30]. Therefore, an ideal glucose biosensor needs to have high sensitivity to glucose but does not have any response to UA and AA. Here is the assessment of the interference study of a glucose biosensor: Fig. S6 shows the responses of GO-Cys-GNR coated active carbon electrode to the solution of glucose at 4 mM, and to the continual addition of AA at 0.125 mM and UA at 0.33 mM. The results showed a maximum of 1.7% of the biosensor current output contributed by the AA and UA at these concentrations. Hence, the

interference of AA and UA to this GO-Cys-GNR coated thick film screen-printed carbon electrode is relatively small and acceptable.

4. Conclusions

3D layer-by-layer graphene-GNR hybrid nanomaterial was synthesized and coated on a thick film screen-printed active carbon of a single use, disposable biosensor. The coating of 3D graphene-GNR layer-by-layer nanostructure on the active carbon electrode enhances the biosensor performance of detecting H_2O_2 through its electro-catalytic reaction. Cyclic voltammetry and amperometry were used to characterize the performances of the biosensor. The mechanism of the performance of the 3D hybrid structure was assessed and the 3D nanostructure increased the contact area of GNR by effectively reducing self-assemblies. The 3D graphene-GNR layer-by-layer modified biosensors showed good response to glucose and with very limited interference by ascorbic acid and uric acid in solution. The technique demonstrated here may become a valuable addition to the catalog of biosensors. A metal nanoparticle with higher catalytic capability such as PtRu [14], will further enhance the selectivity and sensitivity of this biosensor if incorporated into this 3D nanostructure.

Conflict of interest

The authors declare that there is no conflict of interest.

Acknowledgments

This work was supported by the AFOSR–MURI FA 9550-12-1-0037 and AFOSR FA9550-09-1-0254. The TEM data were obtained at the (cryo) TEM facility at the Liquid Crystal Institute, Kent State University, supported by the Ohio Research Scholars Program Research Cluster on Surfaces in Advanced Materials. Technical assistance from the staff of Electronics Design Center of Case Western Reserve University is gratefully acknowledged.

Appendix A. Supplementary data

Supplementary data associated with this article can be found, in the online version, at http://dx.doi.org/10.1016/j.sbsr.2014.10.008.

References

[1] K. Aslan, J.R. Lakowicz, C.D. Geddes, Curr. Opin. Chem. Biol. 9 (2005) 538–544.
[2] S. Chakraborty, C.R. Raj, Biosens. Bioelectron. 24 (2009) 3264–3268.
[3] K.J. Chen, C.F. Lee, J. Rick, S.H. Wang, C.C. Liu, B.J. Hwang, Biosens. Bioelectron. 33 (2012) 75–81.
[4] K.J. Chen, K.C. Pillai, J. Rick, C.J. Pan, S.H. Wang, C.C. Liu, B.J. Hwang, Biosens. Bioelectron. 33 (2012) 120–127.
[5] X.J. Chen, Z.X. Chen, J.W. Zhu, C.B. Xu, W. Yan, C. Yao, Bioelectrochemistry 82 (2011) 87–94.
[6] J.C. Claussen, A.D. Franklin, A. Haque, D.M. Porterfield, T.S. Fisher, ACS Nano 3 (2009) 37–44.
[7] R.S. Dey, C.R. Raj, J. Phys. Chem. C 114 (2010) 21427–21433.
[8] N.J. Durr, T. Larson, D.K. Smith, B.A. Korgel, K. Sokolov, A. Ben-Yakar, Nano Lett. 7 (2007) 941–945.
[9] S.A.G. Evans, J.M. Elliott, L.M. Andrews, P.N. Bartlett, P.J. Doyle, G. Denuault, Anal. Chem. 74 (2002) 1322–1326.
[10] B. Feldman, R. Brazg, S. Schwartz, R. Weinstein, Diabetes Technol. Ther. 5 (2003) 769–779.
[11] R. Guascito, E. Filippo, C. Malitesta, D. Manno, A. Serra, A. Turco, Biosens. Bioelectron. 24 (2008) 1057–1063.
[12] B. Hellman, L.A. Idahl, A. Lernmark, I.B. Taljedal, Proc. Natl. Acad. Sci. U.S.A. 71 (1974) 3405–3409.
[13] S. Hrapovic, Y. Liu, K.B. Male, J.H. Luong, Anal. Chem. 76 (2004) 1083–1088.
[14] C.-C. Kung, P.-Y. Lin, F.J. Buse, Y.H. Xue, X. Yu, L.M. Dai, C.-C. Liu, Biosens. Bioelectron. 52 (2014) 1–7.
[15] J.B. Liu, Y.L. Li, Y.M. Li, J.H. Li, Z.X. Deng, J. Mater. Chem. 20 (2010) 900–906.
[16] E.S. McLamore, S. Mohanty, J. Shi, J.S. Claussen, S. Jedlicka, J.L. Rickus, D.M. Porterfield, J. Neurosci. Methods 189 (2010) 14–22.
[17] E.S. McLamore, J. Shi, D. Jaroch, J.C. Claussen, A. Uchida, Y. Jiang, W. Zhang, S.S. Donkin, M.K. Banks, K. Buhman, K.D. Teegarden, J.L. Rickus, D.M. Porterfield, Biosens. Bioelectron. 26 (2011) 2237–2245.
[18] K.H. Moley, M.M.Y. Chi, M.M. Mueckler, Am. J. Physiol. Endocrinol. Meta. 275 (1998) 38–47.
[19] C.J. Murphy, T.K. San, A.M. Gole, C.J. Orendorff, J.X. Gao, L. Gou, S.E. Hunyadi, T. Li, J. Phys. Chem. B 109 (2005) 13857–13870.
[20] J. Prabhuram, T.S. Zhao, Z.K. Tang, R. Chen, Z.X. Liang, J. Phys. Chem. B 110 (2006) 5245–5252.
[21] J. Shi, E. McLamore, D. Jaroch, J.C. Rickus, D.M. Porterfield, Analyt. Biochem. 411 (2011) 185–193.
[22] J. Shi, H. Zhang, A. Snyder, M.X. Wang, J. Xie, D.M. Porterfield, L.A. Stanciu, Biosens. Bioelectron. 38 (2012) 314–320.
[23] S. Wang, P.-J. Chia, L.-L. Chua, L.-H. Zhao, R.-O. Png, S. Si-varamakrishnan, M. Zhou, R.G.-S. Goh, R.H. Friend, A.T.S. Wee, P.K.-H. Ho, Adv. Mater. 20 (2008) 3440–3446.
[24] H. Wang, Y. Yang, Y. Liang, J.T. Robinson, Y. Li, A. Jackson, Y. Cui, H. Dai, Nano Lett. 11 (2011) 2644–2647.
[25] R.G. Weiss, V.P. Chacko, J.D. Glickson, G. Gerstenblith, Proc. Natl. Acad. Sci. U.S.A. 86 (1989) 6426–6430.
[26] Z.H. Wen, S.Q. Ci, J.H. Li, J. Phys. Chem. C 113 (2009) 13482–13487.
[27] C.M. Xue, O. Birel, M. Gao, S. Zhang, L.M. Dai, A. Urbas, Q. Li, J. Phys. Chem. C 116 (2012) 10396–10404.
[28] C.M. Xue, M. Gao, Y.H. Xue, L. Zhu, L.M. Dai, A. Urbas, Q. Li, J. Phys. Chem. C 118 (2014) 15332–15338.
[29] H.F. Yang, C.S. Shan, F.H. Li, D.X. Han, Q.X. Zhang, L. Niu, Chem. Commun. (2009) 3880–3882.
[30] J.M. You, D. Kim, S. Jeon, Electrochim. Acta 65 (2012) 288–293.
[31] T.J. Zhang, W. Wang, D.Y. Zhang, X.X. Zhang, Y.R. Ma, Y.L. Zhou, L.M. Qi, Adv. Funct. Mater. 20 (2010) 1152–1160.